

Geophysical Research Letters



RESEARCH LETTER

10.1029/2020GL088833

Key Points:

- The zonal mean ITCZ framework is generally not useful for characterizing regional shifts of the tropical rainbelt, regardless of the forcing
- Meridional shifts of the tropical rainbelt vary strongly with longitude under all forcings considered
- All forcings produce robust regional shifts in the rainbelt that are larger than (and sometime oppose the direction of) the zonal mean shift

Supporting Information:

· Supporting Information S1

Correspondence to:

A. R. Atwood, aatwood@fsu.edu

Citation:

Atwood, A. R., Donohoe, A., Battisti, D. S., Liu, X., & Pausata, F. S. R. (2020). Robust longitudinally variable responses of the ITCZ to a myriad of climate forcings. *Geophysical Research Letters*, 47, e2020GL088833. https://doi.org/10.1029/2020GL088833

Received 14 MAY 2020 Accepted 25 JUL 2020 Accepted article online 17 AUG 2020

Robust Longitudinally Variable Responses of the ITCZ to a Myriad of Climate Forcings

Alyssa R. Atwood¹, Aaron Donohoe², David S. Battisti³, Xiaojuan Liu³, and Francesco S. R. Pausata⁴

¹Department of Earth, Ocean, and Atmospheric Science, Florida State University, Tallahassee, FL, USA, ²Polar Science Center, Applied Physics Laboratory, University of Washington, Seattle, WA, USA, ³Department of Atmospheric Sciences, University of Washington, Seattle, WA, USA, ⁴Centre ESCER (Étude et la Simulation du Climat à l'Échelle Régionale) and GEOTOP (Research Center on the dynamics of the Earth System), Department of Earth and Atmospheric Sciences, University of Quebec in Montreal, Montreal, Ouebec, Canada

Abstract We evaluate the longitudinal variation in meridional shifts of the tropical rainbelt in response to natural and anthropogenic forcings using a large suite of coupled climate model simulations. We find that the energetic framework of the zonal mean Hadley cell is generally not useful for characterizing shifts of the rainbelt at regional scales, regardless of the characteristics of the forcing. Forcings with large hemispheric asymmetry such as extratropical volcanic forcing, meltwater forcing, and the Last Glacial Maximum give rise to robust zonal mean shifts of the rainbelt; however, the direction and magnitude of the shift vary strongly as a function of longitude. Even the Pacific rainband does not shift uniformly under any forcing considered. Forcings with weak hemispheric asymmetry such as CO₂ and mid-Holocene forcing give rise to zonal mean shifts that are small or absent, but the rainbelt does shift regionally in coherent ways across models that may have important dynamical consequences.

Plain Language Summary A band of heavy precipitation spanning the deep tropics is an essential feature of the climate system that diverse ecosystems and billions of people depend on. It is well known that this rainbelt, when averaged across all longitudes, shifts north and south in response to heating or cooling the atmosphere in one hemisphere more than the other; this framework has been widely applied to study past tropical rainfall changes under differing climate states. However, we show using many different climate model experiments that this framework does not apply to regional shifts in the rainbelt. Changes in the rainbelt vary from place to place, and thus, data documenting north or south shifts in one location cannot be used to infer similar shifts at other longitudes.

1. Introduction

A large body of literature has emerged over the past two decades demonstrating that there is a latitudinal shift in the distribution of zonally averaged tropical precipitation in response to hemispheric asymmetry in atmospheric heating that is well constrained by energetic arguments (e.g., Chiang & Bitz, 2005; Chiang & Friedman, 2012; Donohoe et al., 2013; Frierson & Hwang, 2012; Kang et al., 2008). This relationship arises because both precipitation and atmospheric energy transport in the tropics are largely controlled by the Hadley circulation: Precipitation occurs in the ascending branch of the Hadley cell, and the cross-equatorial energy transport is proportional to the strength of the Hadley cell at the equator, which is nearly proportional to the distance of the ascending branch from the equator (Lindzen & Hou, 1988). This energetic framework of the zonal mean Hadley cell provides a useful way to relate changes in the tropical climate to the hemispheric-scale energy budget, and thus, shifts in the zonal mean precipitation in idealized and comprehensive model simulations of past, modern, and future climates have been understood in terms of the response to hemispheric asymmetries in atmospheric heating (Broecker & Putnam, 2013; Chiang & Bitz, 2005; Frierson & Hwang, 2012; Hwang et al., 2013; Kang et al., 2008).

Though the energetic framework of the zonal mean Hadley cell has been widely used to assess mechanisms of change in the tropical rainbelt on seasonal to orbital time scales, it obscures the inherently regional nature of tropical rainfall. By construction, it averages out the rich zonal variations of tropical rainfall patterns that reflect the distinct processes that govern the large-scale circulation and precipitation in different regions of

©2020. The Authors.
This is an open access article under the terms of the Creative Commons
Attribution License, which permits use, distribution and reproduction in any medium, provided the original work is properly cited.

ATWOOD ET AL. 1 of 12



the tropics. In particular, the dynamics that govern precipitation in monsoon systems are largely distinct from those that govern precipitation in regions of the ocean characterized by strong sea surface temperature (SST) gradients and narrow rainbands (i.e., the Intertropical Convergence Zones [ITCZs]; e.g., Back & Bretherton, 2006; Biasutti et al., 2018). Shifts in tropical precipitation that occur under interhemispheric changes in atmospheric heating thus tend to be zonally variable, and the heat transport changes have been shown to be of limited utility in explaining local rainfall changes (Adam et al., 2016; Boos & Korty, 2016; Roberts et al., 2017; Singarayer et al., 2017).

Paleoclimate evidence for meridional shifts in tropical rainfall has been found for a variety of past climate states, including the North Atlantic iceberg discharge (Heinrich) events of the last glacial period (Jacobel et al., 2016; Rhodes et al., 2015; Stager et al., 2011; Wang et al., 2001) and the Last Glacial Maximum (LGM, ~21 kyr ago) for which southward shifts of the terrestrial and marine tropical rainbands of up to 7° latitude have been proposed (Arbuszewski et al., 2013; Koutavas & Lynch-Stieglitz, 2004). In addition, a northward shift of the Pacific and Atlantic rainbands of similar magnitude has been proposed during the early-Holocene, when boreal summer insolation was more intense (Jacobel et al., 2016; Haug et al., 2001; Rhodes et al., 2015; Wang et al., 2001). While during the Little Ice Age (LIA, 1400-1850 CE), a southward shift of these rainbands (by up to 5° latitude) has been inferred from proxy records in and around the tropical Pacific and Atlantic (Haug et al., 2001; Lechleitner et al., 2017; Newton et al., 2006; Sachs et al., 2009). Many of these paleoclimate studies have invoked the relationship between the zonal mean position of the ITCZ and the cross-equatorial energy flux (and/or interhemispheric temperature gradient) in interpreting meridional shifts of tropical rainfall. However, it is not clear to what degree proxy data documenting regional shifts in rainfall can be extrapolated to infer similar shifts at other longitudes. In many cases, the large regional shifts proposed from paleoclimate records must be regionally localized (as opposed to zonally homogenous) because the cross-equatorial atmospheric heat transport implied from the zonal mean ITCZ shift of that magnitude is physically untenable (McGee et al., 2014).

In this study, we evaluate the zonal structure of meridional shifts in tropical rainfall in a compilation of climate models under a range of past and future climate forcings. Some forcings are characterized by strong hemispheric asymmetry (e.g., meltwater forcing in the North Atlantic Ocean, extratropical volcanic eruptions, and LGM orography and albedo), while others are characterized by weak hemispheric asymmetry (e.g., quadrupling of CO₂ and mid-Holocene orbital and greenhouse gas forcing). We show that the zonal mean meridional shift of the tropical rainbelt is greater under some forcings than others, but all forcings produce robust regional meridional shifts that are much greater than (and not always in the same direction as) the zonal mean shift.

2. Materials and Methods

2.1. Model Simulations

Details of the all the model simulations used in this study are summarized in Table S1 in the supporting information. LGM and mid-Holocene simulations were taken from the Paleoclimate Modeling Intercomparison Project Phase 2 (PMIP2)/Coupled modeling Intercomparison project Phase 3 (CMIP3) and PMIP3/CMIP5 archives. For the LGM simulations, the forced response was calculated by averaging Years 31–200 after the spin-up period and comparing to the preindustrial (PI) control runs. For the mid-Holocene forcing, the forced response was calculated by averaging Years 100–685 after the spin-up period and comparing to the PI control runs. For the response to CO_2 forcing, we analyzed simulations from the CMIP5 $4xCO_2$ simulations. The forced response was taken to be the difference between the last 50 years of these simulations and the PI control simulations.

Response to volcanic forcing is assessed from selected PMIP3 last millennium (LM) transient simulations (CCSM4 and GISS Model E Ensemble Members 122, 125, and 128), CESM Last Millennium Ensemble (LME) volcanic-only simulations, and an ensemble of simulations with the Norwegian Earth System Model Version 1-M (NorESM) mimicking a high-latitude Northern Hemisphere (NH) summer eruption (the Laki eruption in Iceland; Pausata, Chafik, et al., 2015; Pausata, Grini, et al., 2015). Of the transient LM simulations, CCSM4 and CESM LME prescribed sulfate loading (in Tg) from Gao et al. (2008) and Landrum et al. (2013) (GRA), while GISS 122, GISS 125, and GISS 128 prescribed volcanic aerosols as functions of aerosol optical depth (AOD) and aerosol effective radius with twice the forcing of Crowley

ATWOOD ET AL. 2 of 12



et al. (2008, CEA). While likely overestimating the total volcanic forcing of the LM, the GISS simulations serve as a useful representation of large volcanic events (noting that, in the original CEA data set, AOD during the peak of large volcanic events is substantially lower than that estimated from the GRA data set of sulfate loading; Atwood et al., 2016). To assess the precipitation response to volcanic forcing in these LM runs, years with large extratropical volcanic events were chosen (defined by volcanic events with peak globally averaged AOD > 0.1 and hemispherically averaged AOD at least 25% greater in one hemisphere, where AOD was estimated from the GRA data set by dividing sulfate loading by 150 Tg; Atwood et al., 2016; Stothers, 1984). For each event, the monthly climatology of precipitation was calculated from months with AOD > 0.02 (i.e., 20% of the peak threshold) up to 2 years before and after the peak of the event and compared to the control climatology, which was taken to be the closest 5-year period prior to the onset of the event with minimal volcanic activity (defined as global mean AOD summed over the 5-year period <0.01). These extratropical volcanic events were organized into NH and Southern Hemisphere (SH) volcano composites. In each of the CMIP5 LM and CESM LME simulations, the NH composite consisted of 20 volcanic events, and the SH composite consisted of nine volcanic events that met these criteria. In the NorESM simulations, the Laki eruption was simulated by adding 100 Tg of SO₂ and dust (as an analog for ash) into the upper troposphere and lower stratosphere over a 4-month period, starting on 1 June in a range of years selected from a transient historical (1850-2005) simulation. Forty eight ensemble members were averaged into three composites (each composite therefore consisting of 16 NH eruptions) in order to be consistent with the CMIP5 LM and CESM LME NH composites. The NorESM volcanic forcing runs are compared against their own "No Volcano" control runs that were branched from the same initial conditions of the transient historical simulation.

For the North Atlantic meltwater forcing ("hosing") simulations, an ensemble of simulations with the Community Earth System Model Version 1.0 (CESM 1.0) was used (Atwood, 2015). To simulate the atmospheric response to meltwater-induced terminations of the Atlantic overturning circulation, a set of simulations were branched from the control run with 1 Sv of freshwater forcing imposed across the surface of the northern North Atlantic Ocean (50–70°N) for 100 years. Four ensemble members were performed with this default configuration of CESM by branching from the end of the control run at 9-year intervals. Because it takes 20 years for the Atlantic thermohaline circulation to collapse in these simulations, the last 80 years of the runs are averaged to create the forced climatology.

Additionally, because the default CESM fully coupled control run is known to have large biases in the mean state of the tropical Pacific compared to observations (Figures S1 and S2; Li & Xie, 2014), we also apply the same freshwater forcing to a bias-corrected version of the model. The mean state bias corrections include both a modification to the topography of Central America and surface heat flux modifications, so-called Q-fluxes (also see Zhang et al., 2019). We raised the height of the mountains in Central America to 1,500 m (from 7-18°N, 120-76°W) to reduce the low-level wind biases in the eastern Pacific associated with the poor resolution of Central American topography. Along with the surface heat flux corrections, reductions of these low-level wind biases reduce the SST biases throughout the tropics. In one configuration of the model with three ensemble members we only raised the topography over Central America with no changes in the surface heat fluxes. In a second configuration of the model with four ensemble members we both raise the topography and prescribe a surface heat flux correction with a cyclostationary seasonal cycle throughout the tropical oceans (30°S to 30°N) to further reduce the bias in the climatological seasonal cycle in SST. The mean state bias corrections are described in the supporting information and in Zhang et al. (2019). The tropical surface temperature, precipitation, and wind fields before and after these bias corrections are shown in Figures S1 and S2. The anomalies due to forcing are calculated to be the difference between the final 80 years of each 100-year-long hosing simulations and 100 years of unforced control runs with the same model configuration. We also included two hosing simulations with PMIP2-era models (MPI and HadCM3) in our analyses.

2.2. Changes in the Tropical Precipitation Centroid

Meridional shifts in tropical rainfall are characterized in terms of the mean annual tropical precipitation centroid, P_C (the latitude at which the mean annual area-weighted tropical rainfall to the north equals that to the south, within the bounds 20°N to 20°S). P_C is calculated at each longitude. We decompose forced

ATWOOD ET AL. 3 of 12

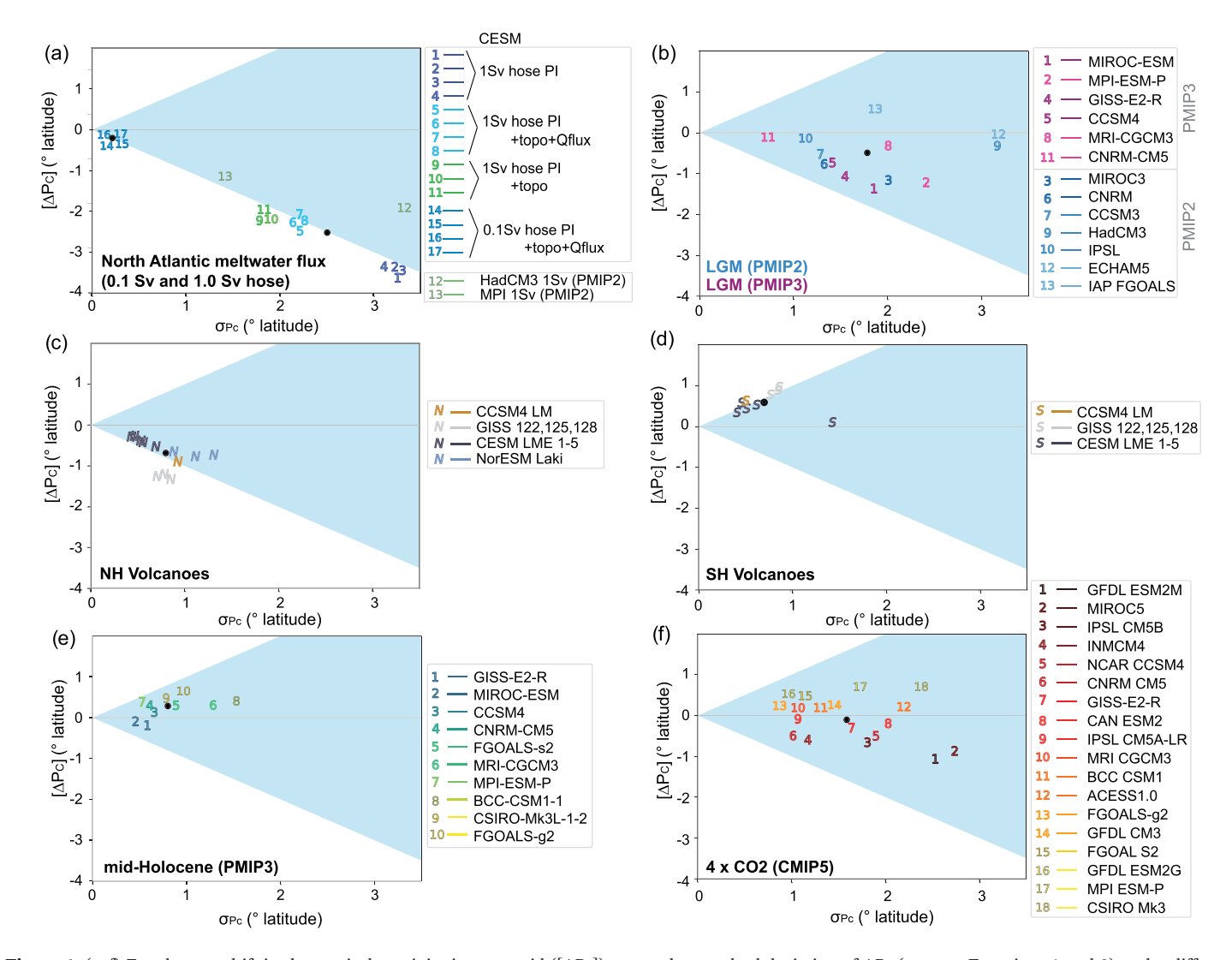


Figure 1. (a–f) Zonal mean shift in the tropical precipitation centroid ($[\Delta P_c]$) versus the standard deviation of ΔP_c (σ_{Pc} ; see Equations 1 and 2) under different climate forcings and boundary conditions. The blue triangle indicates the region where the longitudinal variations in ΔP_c are as large or larger than the zonal mean change in ΔP_c . The black circle indicates the multimodel mean $[\Delta P_c]$ and σ_{Pc} for each forcing type (where the means of the 0.1 and 1.0 Sv meltwater simulations in panel a have been calculated separately).

changes in P_C (ΔP_C ; defined as the difference between a forced simulation and a control simulation) in the following way:

$$\Delta P_{\rm C} = [\Delta P_{\rm C}] + \Delta P_{\rm C}^*, \tag{1}$$

where $[\Delta P_C]$ is the zonal mean change (i.e., ΔP_C averaged over all longitudes) and ΔP_C^* denotes the deviation from the zonal mean. For each set of forcings, in Figure 1 we compare the change in the zonal mean precipitation centroid $[\Delta P_C]$ to the change in the zonal variation of ΔP_C^* (i.e., the "waviness" of ΔP_C), quantifying the latter by the standard deviation of ΔP_C (which is identically the standard deviation of ΔP_C^*) across longitudes:

$$\sigma_{Pc} = \left(\frac{1}{N-1} \sum_{j=1}^{N} (\Delta P_{C} - [\Delta P_{C}])^{2}\right)^{1/2} = \left(\frac{1}{N-1} \sum_{j=1}^{N} (\Delta P_{C}^{*})^{2}\right)^{1/2}, \tag{2}$$

where j = all longitudes. To evaluate the robustness of regional shifts in the precipitation centroid across models, changes in P_C were discretized into zonal bins of width 15° longitude.

ATWOOD ET AL. 4 of 12



Table 1Zonal Mean and Zonal Variation in Meridional Shifts of the Precipitation Centroid Under Different Forcings

	0 0	*	00				
				Forcing type			
						Mid-	
Centroid metrics	Volcanic (NH)	Volcanic (SH)	Hosed (1 Sv)	Hosed (0.1 Sv)	LGM	Holocene	4xCO ₂
$[\Delta P_c]$ (multimodel mean \pm standard error) ^a	-0.72 ± 0.10	0.59 ± 0.09	-2.48 ± 0.02	-0.23 ± 0.03	-0.53 ± 0.15	0.27 ± 0.08	-0.07 ± 0.12
σ_{Pc} (multimodel mean \pm standard error) ^a	0.77 ± 0.07	0.71 ± 0.10	2.45 ± 0.18	0.23 ± 0.02	1.84 ± 0.20	0.82 ± 0.10	1.61 + 0.13
# models with northward shift of $[\Delta P_c]$	0/12	9/9	0/13	0/4	1/13	8/10	9/18
# models with southward shift of $[\Delta P_c]$	12/12	0/9	13/13	4/4	12/13	2/10	9/18
3- 1 2 1 0 1 1							

^aSee section 2.2 for definitions.

3. Results and Discussion

3.1. How Does the Zonal Mean Shift of the Rainbelt Compare to the Zonal Variations?

The zonal mean shift of the tropical rainbelt is robust across models under climate forcings with strong hemispheric asymmetry. The zonal mean rainbelt shifts south in all models under North Atlantic meltwater forcing, NH extratropical volcanic eruptions, and in the majority of models (12/13) under LGM boundary conditions (ordinate of Figures 1a-1c and Table 1). These shifts are expected due to the hemispheric asymmetry in atmospheric heating associated with the slowdown of the Atlantic thermohaline circulation and Arctic sea ice growth in the case of North Atlantic meltwater forcing, the scattering of solar radiation in the NH by stratospheric sulfate aerosols in the case of NH volcanic eruptions, and the presence of large, high albedo NH ice sheets in the case of the LGM. Similarly, the zonal mean rainbelt shifts robustly north under SH extratropical volcanic eruptions (Figure 1d) and weakly north in most models (8/10) under mid-Holocene boundary conditions (Figure 1e). Only under CO₂ forcing is there no robust ensemble mean shift of the zonal mean rainbelt (Figure 1f). In one of the five CESM LME ensemble members (LME 2), the SH volcano composite exhibits a markedly different precipitation response to the other four ensemble members (and to the four GISS and CCSM4 LM simulations; Figure 1d). In this simulation, the SH volcanic events produce a weaker northward shift of the zonal mean precipitation centroid and larger zonal variation in the shift as compared to the other ensemble members. This anomalous response is due to the fact that six out of the nine SH volcanic events in this simulation occur during moderate to strong El Niño events (defined as five consecutive 3-month running mean Niño 3.4 SST anomalies at or above +1.0°C), which is substantially more than the zero to three events for the other ensemble members. Because the forced precipitation response to SH volcanoes in this simulation is overwhelmed by tropical Pacific SST variability, we omit this ensemble member from the remainder of our analyses.

There are large longitudinal variations in ΔP_C under all forcings considered, including those forcings that give rise to large zonal mean shifts of the rainbelt and those that do not. To quantify the zonal mean shift of the rainbelt relative to its zonal variation in each set of simulations, the amplitude of the zonal mean change in the tropical precipitation centroid ($[\Delta P_C]$) is compared to the standard deviation of ΔP_C across longitudes (σ_{Pc} ; Figure 1). In this plane of P_C changes, data points that fall within the blue shaded sector in Figure 1 indicate changes in tropical precipitation that are more zonally inhomogeneous than they are zonally homogeneous, whereas regions in white represent tropical precipitation changes that are more zonally homogenous. Under no forcing is the zonal mean shift substantially larger than the zonal variation (1σ) in the shift, as indicated by the changes in ΔP_C falling near or within the blue shaded sector. Of all the forcings considered, shifts in the mean position of the rainbelt are largest (up to 3.5° latitude) when there is a sufficiently large North Atlantic meltwater forcing to cause a collapse in the Atlantic Meridional Overturning Circulation (Figure 1a). However, even in this extreme scenario, the zonal variation (1σ) in the shift is as large as the zonal mean shift, across individual simulations and in the multimodel mean. Notably, the zonal mean shift and zonal variations are much larger in the CESM simulations without any bias corrections than those with bias corrections (cf. simulations 1-4 vs. 5-11 in Figure 1a). A similar relationship between the zonal mean shift and the zonal variations is observed under extratropical volcanic forcing (i.e., near 1:1 scaling): Although the amplitude of the response is far more muted than the

ATWOOD ET AL. 5 of 12

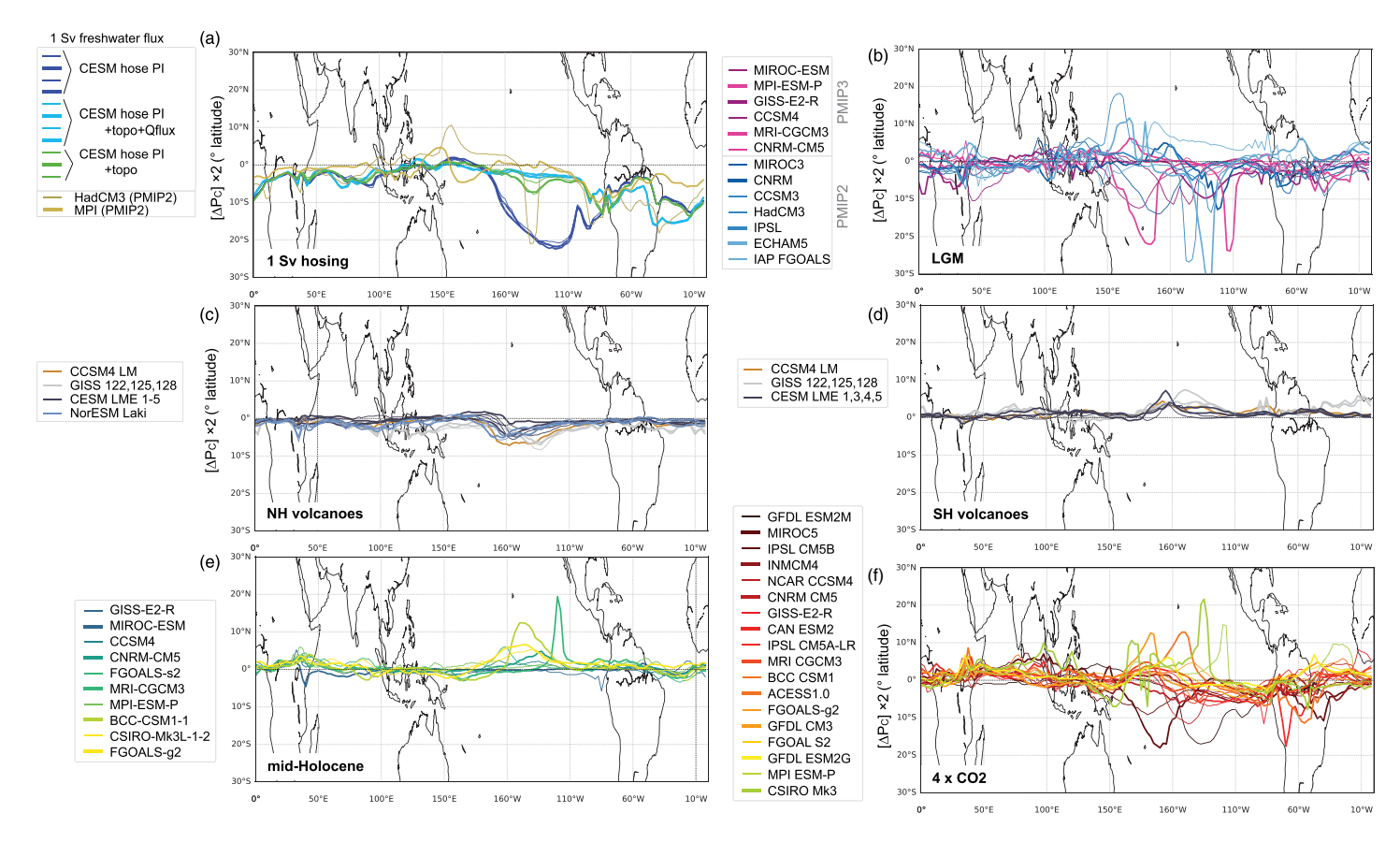


Figure 2. (a-f) The meridional shift in the tropical precipitation centroid $(2 \times \Delta P_c)$ as a function of longitude under different climate forcings and boundary conditions. The meridional displacement has been multiplied by a factor of 2 for visual clarity.

response to meltwater forcing, the zonal variation in the shift is also of similar magnitude to the zonal mean shift (Figures 1c and 1d).

In contrast to the meltwater and volcanic forcing simulations, under all other forcings considered, the zonal variations in ΔP_C are generally much larger than the zonal mean ΔP_C . In the LGM simulations, the zonal variations in ΔP_C range from 0.7° to 3.2° latitude, with some models exhibiting as much zonal variation as that found in the 1 Sv North Atlantic meltwater simulations (1.4 $\leq \sigma_{PC} \leq$ 3.3° latitude; Figures 1a and 1b). However, the zonal mean shift in the LGM (multimodel mean and standard error in $[\Delta P_C] = -0.5 \pm 0.2^\circ$ latitude) is on average much smaller than that which occurs in response to meltwater forcing (-2.5 \pm 0.2° latitude; cf. ordinate values in Figure 1a vs. Figure 1b). There is, however, general agreement in the sign of the zonal mean shift in the LGM simulations: in 6/7 of the PMIP2 models and all of the PMIP3 models, the zonal mean ITCZ shifts southward by up to 1.4° latitude. Notably, the more recent PMIP3 LGM simulations demonstrate a greater zonal mean shift and less zonal variation on average as compared to their PMIP2 counterparts (Figure 1b); the differences between these two classes of models are most pronounced in the tropical Pacific, where several PMIP2 models demonstrate a northward shift of tropical precipitation in parts of the region (Figure 2b).

Under mid-Holocene conditions, zonal variations in ΔP_C are on average much smaller than in the LGM simulations (multimodel mean and standard error in $\sigma_{Pc}=0.8\pm0.1^\circ$ latitude vs. $1.8^\circ\pm0.2^\circ$ latitude, respectively; Figures 1e and 1b and Table 1). While the zonal mean shift is also small under mid-Holocene forcing ([ΔP_C] = $0.3\pm0.1^\circ$ latitude), there is general consistency in the northward direction of the shift (8/10 models). In contrast, under abrupt $4xCO_2$ forcing, zonal variations in ΔP_C are generally as large as under LGM conditions (multimodel mean $\sigma_{Pc}=1.6^\circ\pm0.1^\circ$ latitude versus $1.8^\circ\pm0.2^\circ$ latitude, respectively) and the zonal variations far exceed the magnitude of the zonal mean ΔP_C in every model (i.e., all points are well

ATWOOD ET AL. 6 of 12

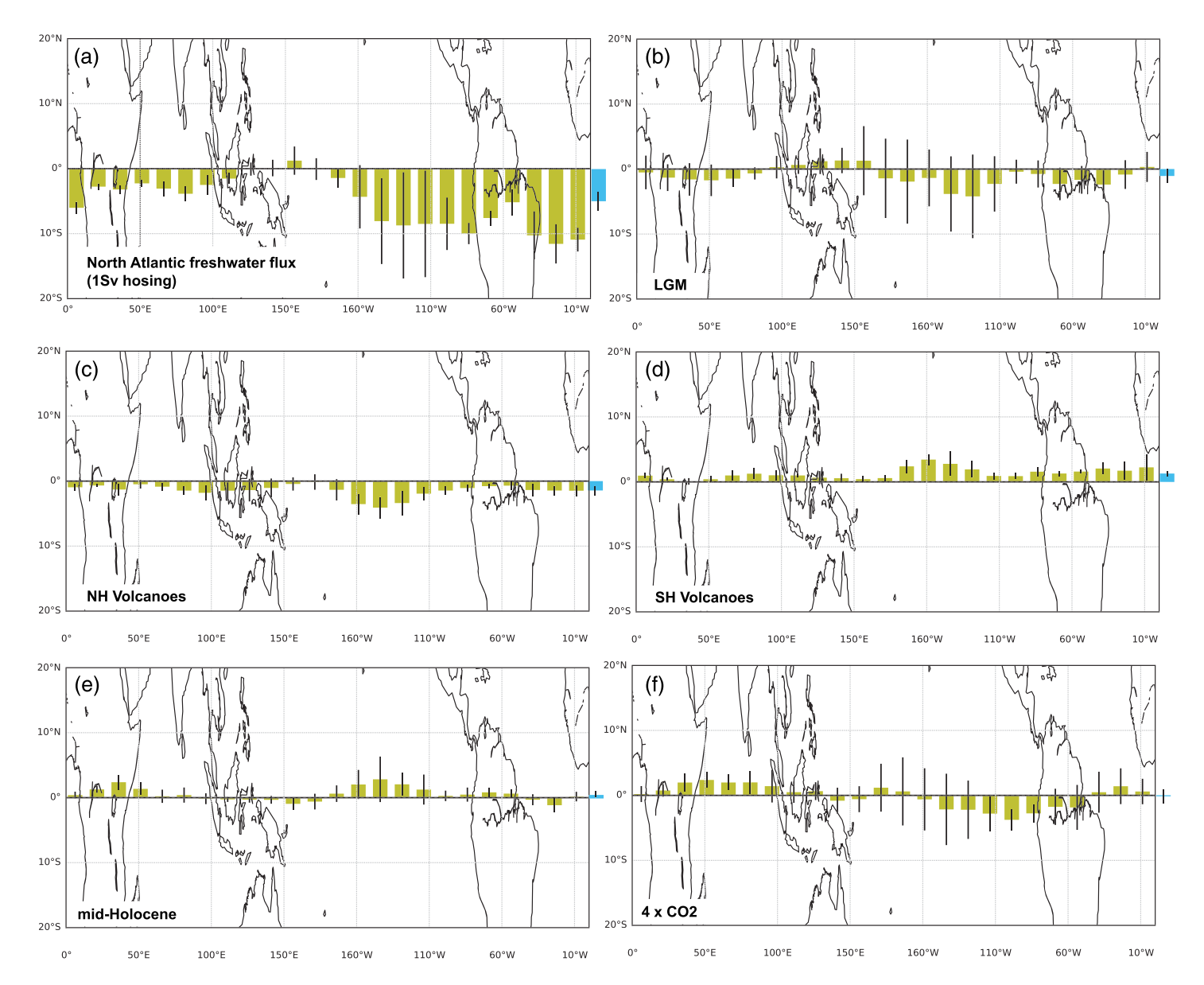


Figure 3. (a–f) Change in tropical precipitation centroid (ΔP_c) as a function of longitude under different climate forcings and boundary conditions. Yellow bars indicate the multimodel mean ΔP_c (multiplied by a factor of 2 for visual clarity) averaged over zonal bins of width 15° longitude. The whiskers represent $\pm 1\sigma$ across models. Blue bars indicate the multimodel mean zonally averaged ΔP_c ([P_c]), also multiplied by a factor of 2 for visual clarity.

within the blue sector in Figure 1f). Additionally, there is no consistency in the direction of the zonal mean shift under CO₂ forcing (northward in 9/18 models and southward in 9/18 models). However, the rainbelt does shift regionally in coherent ways across models, as described in section 3.2.

3.2. Where Are There Robust Regional Shifts of the Rainbelt?

We now assess whether robust regional variations of the rainbelt occur in response to a given forcing. These investigations are important because in places where tropical rainfall shifts systematically across all models, this suggests that a robust set of physical mechanisms underlie the rainfall response in those regions. Furthermore, identifying where robust regional variations of the rainbelt occur in response to a given forcing is important for understanding the globally teleconnected response of the climate system to that forcing, as the regional rainfall changes in the tropics dictate tropical and extratropical teleconnection patterns (through latent heating of the atmosphere) and give rise to regional ocean-atmosphere feedbacks such as

ATWOOD ET AL. 7 of 12



the Bjerknes feedback (e.g., Gill, 1980; Trenberth et al., 2002; Wallace et al., 1998). To assess the robustness of the regional shifts in the precipitation centroid under each type of forcing, we compare the multimodel mean ΔP_C in discretized zonal bins to the standard deviation of ΔP_C around the multimodel mean (i.e., $\pm 1\sigma$ across models) in Figure 3.

Under North Atlantic meltwater forcing, the rainbelt shifts south robustly across models at all longitudes except for the western Pacific and Maritime Continent (Figure 3a), although there is substantial longitudinal variation in the magnitude of the shift, as noted above for individual models. A large systematic southward shift occurs in the Atlantic and eastern Pacific Oceans (4-6° latitude) and to a lesser degree over the Indian Ocean and Africa (2.5° latitude). Little to no shift of the rainbelt occurs over the western Pacific, while the shift over the Indian Ocean and Africa is most similar to the zonal mean (2.5° latitude). These features of the annual mean rainbelt response also generally apply to the seasonal climatologies (Figure S3), though several distinct features arise in the seasonal responses, including an enhanced southward shift of the eastern Pacific rainbelt during boreal winter and spring and a subtle but coherent northward shift in the western Pacific in boreal summer. The longitudinal extent and location of the annual mean shift in the Pacific rainband vary widely between models, with the largest intermodel variation in ΔP_C occurring in the central Pacific, where the precipitation centroid is particularly sensitive to changes in the location and intensity of the northern and southern branches of the Pacific ITCZ. In this region, as well as in the eastern Pacific and Atlantic sectors, the response strongly depends on whether or not the model has been flux corrected to have a more realistic climatology (Figures 2a and S1). In particular, the southward precipitation shift is greater in the Atlantic but smaller in the Pacific in the bias-corrected versions of CESM, as compared to their non-bias-corrected counterparts. More specifically, the precipitation response increases in the Atlantic when the surface heat flux correction is added (which sharpens the Atlantic rainband; Figures S1b and S1c), while the precipitation response decreases in the Pacific when Central American topography is raised (with and without the surface heat flux correction, as the eastern Pacific low level winds become less responsive to changes in the tropical Atlantic). These bias-corrected meltwater simulations demonstrate the sensitivity of the rainfall response to the background climate state in the tropics underscoring the importance of model development efforts to improve the representation of tropical rainfall climatology, as models with biased mean states are likely to yield biased estimates of the rainfall response to forcing. Furthermore, our suite of simulations suggests that the atmospheric communication of ITCZ shifts between the Atlantic and Pacific basins is most impacted by the specification of topography, with raised topography across Central America inhibiting the connection between these ocean basins.

Under volcanic forcing, the longitudinal structure of the precipitation shift is nearly equal and opposite between the NH and SH eruptions. The amplitude of the zonal mean shift is 0.5–1.0° latitude, similar to the regional shifts over the Atlantic and eastern Indian Oceans and parts of the Maritime Continent (Figures 3c and 3d). Larger systematic shifts of 1–2° occur in the central Pacific, which are most pronounced in boreal winter (Figures S4 and S5). The annual mean shift is generally weaker over land than ocean regions, with the exception of the western Pacific; as with North Atlantic meltwater forcing, the precipitation centroid over the western Pacific is insensitive to volcanic forcing.

Under LGM boundary conditions, 12/13 models demonstrate a southward shift of tropical precipitation in the zonal mean, though the zonal variations are typically much larger than the small zonal mean shift of $-0.5^{\circ} \pm 0.2^{\circ}$ latitude (Table 1 and Figure 1b), consistent with the findings of Roberts, Valdes, and Singarayer (Roberts et al., 2017). The models tend to diverge widely in their regional representation of the rainbelt response in most regions (Figures 2b and 3b), with the largest intermodel variations appearing in the central and western Pacific (where ΔP_C varies from 9° north to 15° south across models; Figure 2b). However, in most models, rainfall shifts south over South America, with all seasons contributing roughly equally to the annual mean response (Figures 3b and S6), and rainfall also shifts south over East Africa and the western Indian Ocean (primarily in boreal summer and fall). It is these regions, as well as a large southward shift in the central Pacific in some models, that drive the southward zonal mean ITCZ shift in the LGM simulations. Over the Maritime Continent, where rainfall shifts are typically weak under most forcings, seasonal changes in the pattern of large-scale drying in the region drive large and coherent seasonal shifts in the precipitation centroid (data not shown). However, because these seasonal shifts tend to

ATWOOD ET AL. 8 of 12



cancel one another (northward during boreal spring and summer and southward in boreal winter; Figure S6), the annual mean response over the Maritime Continent is weak.

In contrast to the North Atlantic meltwater, volcanic, and LGM simulations, the mid-Holocene and 4xCO₂ simulations are characterized by weak interhemispheric asymmetry in their prescribed forcings. Under mid-Holocene conditions, 8/10 models demonstrate a weak northward shift of zonal mean tropical rainfall, though the zonal variations are substantially larger than the small zonal mean shift, which is only $0.3^{\circ} \pm 0.1^{\circ}$ latitude in the multimodel mean (Table 1 and Figure 1e). In most models, this zonal mean shift is driven by northward shifts of rainfall over the central Pacific and East Africa, while a weak southward shift (opposing the zonal mean) typically occurs over the tropical Atlantic (Figure 3e). The mid-Holocene rainbelt changes display large seasonal variations (Figure S7), in association with the large seasonal changes in insolation that arise under precessional forcing (with more intense insolation during boreal summer and less intense insolation during austral summer, relative to today). For example, in boreal summer a prominent northward shift in rainfall occurs over the Atlantic Ocean and Africa, associated with enhanced NH summer monsoons. Austral summer, in contrast, is characterized by a weakening of the South American summer monsoon and an associated northward shift in the precipitation centroid at those longitudes. Over the Atlantic and Pacific Oceans, the rainbands shift in opposite directions (north over the central Pacific and south over the tropical Atlantic), most prominently in boreal winter and spring (December-February [DJF] and March-May [MAM]; Figure S7), which leads to a weakly opposing pattern in the annual mean response (Figure 3e).

 CO_2 forcing gives rise to the largest zonal variations of any forcing considered and no robust zonal mean precipitation shift (Figures 1f and 2f). This is because there are robust and opposing *regional* shifts in tropical precipitation (Figure 3f). The rainfall distribution robustly shifts southward in the eastern Pacific and shifts northward by a similar magnitude over the Indian Ocean and East Africa. We emphasize that the direction of these regional shifts in the rainbelt is robust across models despite the wildly diverging direction of the zonal mean rainbelt shift. These robust regional shifts are manifested in different seasons—while the eastern Pacific shift is most pronounced in boreal winter, the shift over the Indian Ocean and East Africa is most pronounced in boreal fall (Figure S8). As with most other forcings, the precipitation centroid over the western Pacific and Maritime Continent is insensitive to CO_2 forcing, while shifts in the central Pacific are large but vary widely across models (Figures 2f and S8).

Considering all forcings in aggregate, the largest shifts of the tropical precipitation centroid tend to occur in the central and eastern Pacific, where this metric is particularly sensitive to changes in the intensity and location of the northern and southern branches of the Pacific ITCZ. However, models also tend to differ widely in their rainfall response to forcing over this region. Tropical mean state biases appear to be a major culprit of the disparate central and eastern Pacific rainfall responses (as indicated by bias-corrected versions of the meltwater simulations), thus highlighting an important caveat to interpreting rainfall changes in this region from model simulations with poor representation of tropical rainfall climatology.

Finally, it is clear from all of the forcings analyzed in this study that ΔP_C in the central and eastern Pacific is not simply related to ΔP_C in the western Pacific (Figure 3). As shown in Figure 2, the Pacific rainband does not shift uniformly across all longitudes under any forcing considered, even within a single model. Under forcings with large hemispheric asymmetry, shifts of the central and eastern Pacific rainband tend to be coordinated with shifts of the Atlantic rainband but are largely decoupled from the western Pacific, where the response of the annual mean precipitation centroid is weak under any forcing considered (Figures 3a–3f). When robust shifts of the zonal mean rainbelt occur, the central and eastern Pacific provide the greatest contribution to the zonal mean shift. These results highlight the importance of capturing this region when attempting to reconstruct the sign of a change in the zonal mean Hadley circulation from the paleoclimate record (subject to the caveats regarding mean state biases discussed above).

4. Conclusions

In response to a variety of natural and anthropogenic forcings, we find that the magnitude and direction of meridional shifts of the tropical rainbelt vary strongly with longitude. Analysis of a large suite of model simulations demonstrates that the zonal mean framework is generally not useful for characterizing shifts at regional scales regardless of the type of forcing. Forcings with large hemispheric asymmetry (including

ATWOOD ET AL. 9 of 12



extratropical volcanic eruptions, meltwater forcing in the North Atlantic Ocean, and the LGM) give rise to robust zonal mean shifts of the rainbelt; however, the direction and magnitude of the shift vary strongly as a function of longitude. Under forcings with weak hemispheric asymmetry (including CO_2 quadrupling and mid-Holocene insolation and greenhouse gas forcing), zonal mean shifts are small or absent, but robust regional shifts occur that may have important dynamical consequences.

Considering all forcings analyzed in this study, it is notable that even the tropical Pacific rainband does not shift uniformly under any forcing. The rainband location over the western Pacific and Maritime Continent is relatively insensitive to most types of forcing, while meridional shifts of the central and eastern Pacific rainband tend to be coordinated with the Atlantic rainband under forcings with large hemispheric asymmetry. When robust shifts of the zonal mean rainband occur, the central and eastern Pacific provide the greatest contribution to the zonal mean shift, highlighting the importance of capturing this region when attempting to constrain the sign of the zonal mean Hadley cell change based on networks of paleoclimate data. These findings demonstrate the zonal complexity inherent in shifts in the tropical rainbelt and caution against the practice of inferring large-scale (i.e., Pacific basin wide and larger) changes in the tropical rainbelt based on data from a limited spatial domain.

Despite the longitudinally variable rainband responses, under each type of forcing, we find regional shifts in the tropical rainbelt that are robust across models. These robust responses suggest that there may be a robust set of physical mechanisms that drive the regional rainfall shifts. For example, under North Atlantic meltwater forcing, a large systematic southward shift (4-6° latitude) of the tropical rainbelt occurs in the Atlantic and eastern Pacific Oceans, presumably in response to the large changes in the meridional SST gradient in these regions (Atwood, 2015). However, many other systematic features in the regional rainband responses to forcing are not well understood and warrant further study, such as those produced by LGM boundary conditions, where a modest but robust southward shift of zonal mean rainfall arises from regional rainfall shifts over the central Pacific, South America, and East Africa/western Indian Ocean. Also deserving of further investigation are the regional rainband responses to CO₂ forcing, featuring a robust southward shift in tropical rainfall over the eastern Pacific Ocean and a northward shift by a similar magnitude over the Indian Ocean and East Africa. CO₂ forcing in particular highlights the limitations of the zonal mean framework wherein the lack of a robust zonal mean shift across models obscures robust regional shifts of opposing direction. These robust regional responses should be evaluated against the proxy record where possible, as, using one model, we have shown that the regional response to forcing can be very sensitive to model biases in the climatological mean state to which the forcing is applied (cf. the response of the CESM, with and without bias corrections, to meltwater forcing; Figures 1a and 2a). Hence, in the cases where there are systematic, common biases across models (e.g., double ITCZs in the tropical Pacific), the efficacy of a robust regional precipitation response to forcing is unclear.

We have shown that the regional rainfall changes under forcing are not simply related to the zonal mean rainfall changes. Thus, the energetic theory that accounts for shifts in the zonal mean ITCZ cannot be applied to regional scales, and hence, new theory is required to explain how local rainfall changes can be placed into the global context. While an analysis of the accompanying energy fluxes is outside the scope of this study, it is likely that such theoretical frameworks need to account for zonal and meridional moist static energy transports by stationary (and possibly transient) eddies, in addition to the mean meridional circulation, as previous work has shown the importance of these processes on the regional rainfall response to forcing (Boos & Korty, 2016; Roberts et al., 2017).

Data Availability Statement

The model precipitation data used in this study were uploaded to Figshare and published with the following doi (10.6084/m9.figshare.12284282). All CMIP5/PMIP3 and CMIP3/PMIP2 climate model data were downloaded from the Earth System Grid Federation (ESGF) node hosted by Lawrence Livermore National Laboratory data repositories (https://esgf-node.llnl.gov/).

References

Adam, O., Bischoff, T., & Schneider, T. (2016). Seasonal and interannual variations of the energy flux equator and ITCZ Part II: Zonally varying shifts of the ITCZ. *Journal of Climate*, 29, 7281–7293.

Acknowledgments

The authors gratefully acknowledge all those who made the CMIP5/PMIP3 and CMIP3/PMIP2 model data open for public access and the many modeling groups who participated in those projects. The authors thank A. Timmermann for providing data from the MPI and HadCM3 meltwater forcing simulations. This material is based upon work supported by the National Science Foundation Paleo Perspective on Climate Change (P2C2) Grant AGS-1702827 awarded to A. D. and A. R. A. Support was provided to D. S. B. and X. L. by grants from the National Science Foundation (Division of Earth Sciences Continental Dynamics Programs Award 1210920 and Frontiers in Earth System Dynamics Award 1338694). Support was also provided to D. S. B by the Tamaki Foundation. F. S. R. P. acknowledges the financial support from the Natural Sciences and Engineering Research Council of Canada (Grant RGPIN-2018-04981) and the Fonds de recherche du Québec-Nature et technologies (2020-NC-268559). We would like to acknowledge C. M. Bitz for assistance in developing the bias-corrected CESM simulations and the high-performance computing support from Cheyenne (doi:10.5065/ D6RX99HX) provided by NCAR's Computational and Information Systems Laboratory, sponsored by the National Science Foundation. The NorESM climate model simulations were performed on resources provided by the Swedish National Infrastructure for Computing at the National

Supercomputer Centre.

ATWOOD ET AL. 10 of 12



- Arbuszewski, J. A., de Menocal, P. B., Cleroux, C., Bradtmiller, L., & Mix, A. (2013). Meridional shifts of the Atlantic Intertropical Convergence Zone since the Last Glacial Maximum. *Nature Geoscience*, 6, 959–962.
- Atwood, A. R. (2015). Mechanisms of tropical Pacific climate change during the Holocene. (PhD thesis, pp. 1–198). University of Washington. Atwood, A. R., Battisti, D. S., Wittenberg, A. T., Roberts, W. H. G., & Vimont, D. J. (2016). Characterizing unforced multi-decadal variability of ENSO: A case study with the GFDL CM2.1 coupled GCM. Journal Climate, 29, 1161–1178.
- Back, L. E., & Bretherton, C. S. (2006). Geographic variability in the export of moist static energy and vertical motion profiles in the tropical Pacific. *Geophysical Research Letters*, 33, L17810. https://doi.org/10.1029/2006GL026672
- Biasutti, M., Voigt, A., Boos, W. R., Braconnot, P., Hargreaves, J. C., Harrison, S. P., et al. (2018). Global energetics and local physics as drivers of past, present and future monsoons. *Nature Geoscience*, 11(6), 392–400. https://doi.org/10.1038/s41561-018-0137-1
- Boos, B. R., & Korty, R. L. (2016). Regional energy budget control of the Intertropical Convergence Zone and application to mid-Holocene rainfall. *Nature Geoscience*, 9(12), 892–897. https://doi.org/10.1038/ngeo2833
- Broecker, W. S., & Putnam, A. E. (2013). Hydrologic impacts of past shifts of Earth's thermal equator offer insight into those to be produced by fossil fuel CO₂. Proceedings of the National Academy of Sciences, 110(42), 16710–16715. https://doi.org/10.1073/pnas.1301855110
- Chiang, J. C. H., & Bitz, C. M. (2005). Influence of high latitude ice cover on the marine Intertropical Convergence Zone. *Climate Dynamics*, 25(5), 477–496. https://doi.org/10.1007/s00382-005-0040-5
- Chiang, J. C. H., & Friedman, A. R. (2012). Extratropical cooling, interhemispheric thermal gradients, and tropical climate change. Annual Review of Earth and Planetary Sciences, 40(1), 383–412. https://doi.org/10.1146/annurev-earth-042711-105545
- Crowley, T. J., Zielinski, G., Vinther, B., Udisti, R., Kreutz, K., Cole-Dai, J., & Castellano, E. (2008). Volcanism and the Little Ice Age. *PAGES Newsletter*, 16(2), 22–23. https://doi.org/10.22498/pages.16.2.22
- Donohoe, A., Marshall, J., Ferreira, D., & McGee, D. (2013). The relationship between ITCZ location and cross-equatorial atmospheric heat transport: From the seasonal cycle to the last glacial maximum. *Journal of Climate*, 26(11), 3597–3618. https://doi.org/10.1175/JCLI-D-12-00467.1
- Frierson, D. M. W., & Hwang, Y. T. (2012). Extratropical influence on ITCZ shifts in slab ocean simulations of global warming. *Journal of Climate*, 25(2), 720–733. https://doi.org/10.1175/JCLI-D-11-00116.1
- Gao, C., Robock, A., & Ammann, C. (2008). Volcanic forcing of climate over the past 1500 years: An improved ice core-based index for climate models. *Journal of Geophysical Research*, 113, D231111. https://doi.org/10.1029/2008JD010239
- Gill, A. E. (1980). Some simple solutions for heat-induced tropical circulation. Quarterly Journal of the Royal Meteorological Society, 106(449), 447–462. https://doi.org/10.1002/qj.49710644905
- Haug, G. H., Hughen, K. A., Sigman, D. M., Peterson, L. C., & Rohl, U. (2001). Southward migration of the Intertropical Convergence Zone through the Holocene. Science, 293(5533), 1304–1308. https://doi.org/10.1126/science.1059725
- Hwang, Y. T., Frierson, D. M. W., & Kang, S. M. (2013). Anthropogenic sulfate aerosol and the southward shift of tropical precipitation in the late 20th century. *Geophysical Research Letters*, 40, 1–6. https://doi.org/10.1002/grl.50502
- Jacobel, A. W., McManus, J. F., Anderson, R. F., & Winckler, G. (2016). Large deglacial shifts of the Pacific Intertropical Convergence Zone.

 Nature Communications 7
- Kang, S. M., Held, I. M., Frierson, D. M. W., & Zhao, M. (2008). The response of the ITCZ to extratropical thermal forcing: Idealized slab-ocean experiments with a GCM. *Journal of Climate*, 21(14), 3521–3532. https://doi.org/10.1175/2007JCLI2146.1
- Koutavas, A., & Lynch-Stieglitz, J. (2004). Variability of the marine ITCZ over the eastern Pacific during the past 30,000 years: Regional perspective and global context. In R. B. A. H. Diaz (Ed.), *The Hadley circulation: Present, past and future, Advances in Global Change Research* (Vol. 21, pp. 347–369). Dordrecht, The Netherlands: Springer. https://doi.org/10.1007/978-1-4020-2944-8_13
- Landrum, L., Otto-Bliesner, B. L., Wahl, E. R., Conley, A., Lawrence, P. J., Rosenbloom, N., & Teng, H. (2013). Last millennium climate and its variability in CCSM4. *Journal of Climate*, 26(4), 1085–1111. https://doi.org/10.1175/JCLI-D-11-00326.1
- Lechleitner, F. A., Breitenbach, S. F. M., Rehfeld, K., Ridley, H. E., Asmerom, Y., Prufer, K. M., et al. (2017). Tropical rainfall over the last two millennia: evidence for a low-latitude hydrologic seesaw. *Scientific Reports*, 7(1), 45809. https://doi.org/10.1038/srep.45809
- Li, G., & Xie, S.-P. (2014). Tropical biases in CMIP5 multimodel ensemble: The excessive equatorial Pacific cold tongue and double ITCZ problems. *Journal of Climate*, 27(4), 1765–1780. https://doi.org/10.1175/JCLI-D-13-00337.1
- Lindzen, R. S., & Hou, A. Y. (1988). Hadley circulations for zonally averaged heating centered off the equator. *Journal of the Atmospheric Sciences*, 45(17), 2416–2427. https://doi.org/10.1175/1520-0469(1988)045%3C2416:HCFZAH%3E2.0.CO;2
- McGee, D., Donohoe, A., Marshall, J., & Ferreira, D. (2014). Changes in ITCZ location and cross-equatorial heat transport at the Last Glacial Maximum, Heinrich Stadial 1, and the mid-Holocene. *Earth and Planetary Science Letters*, 390, 69–79. https://doi.org/10.1016/j.epsl.2013.12.043
- Newton, A., Thunell, R., & Stott, L. (2006). Climate and hydrographic variability in the Indo-Pacific Warm Pool during the last millennium. Geophysical Research Letters, 33, L19710. https://doi.org/10.1029/2006GL027234
- Pausata, F. S. R., Chafik, L., Caballero, R., & Battisti, D. S. (2015). Impacts of high-latitude volcanic eruptions on ENSO and AMOC. Proceedings of the National Academy of Sciences, 112.
- Pausata, F. S. R., Grini, A., Caballero, R., Hannachi, A., & Seland, O. (2015). High-latitude volcanic eruptions in the Norwegian Earth System Model: the effect of different initial conditions and of the ensemble size. *Tellus B: Chemical and Physical Meteorology*, 67.
- Rhodes, R. H., Brook, E. J., Chiang, J. C. H., Blunier, T., Maselli, O. J., McConnell, J. R., et al. (2015). Enhanced tropical methane production in response to iceberg discharge in the North Atlantic. Science, 348(6238), 1016–1019. https://doi.org/10.1126/ science.1262005
- Roberts, W. H. G., Valdes, P. J., & Singarayer, J. S. (2017). Can energy fluxes be used to interpret glacial/interglacial precipitation changes in the tropics? *Geophysical Research Letters*, 44, 6373–6382. https://doi.org/10.1002/2017GL073103
- Sachs, J. P., Sachse, D., Smittenberg, R. H., Zhang, Z., Battisti, D. S., & Golubic, S. (2009). Southward movement of the Pacific Intertropical Convergence Zone AD 1400-1850. Nature Geoscience, 2(7), 519–525. https://doi.org/10.1038/ngeo554
- Singarayer, J. S., Valdes, P. J., & Roberts, W. H. G. (2017). Ocean dominated expansion and contraction of the late Quaternary tropical rainbelt. *Scientific Reports*, 7(1), 9382. https://doi.org/10.1038/s41598-017-09816-8
- Stager, J. C., Ryves, D. B., Chase, B. M., & Pausata, F. S. R. (2011). Catastrophic drought in the Afro-Asian monsoon region during Heinrich event 1. Science, 331(6022), 1299–1302. https://doi.org/10.1126/science.1198322
- Stothers, R. B. (1984). The great Tambora eruption in 1815 and its aftermath. Science, 224(4654), 1191–1198. https://doi.org/10.1126/science.224.4654.1191
- Trenberth, K. E., Caron, J. M., Stepaniak, D. P., & Worley, S. (2002). Evolution of El Nino-Southern Oscillation and global atmospheric surface temperatures. *Journal of Geophysical Research*, 107(D8), 4065. https://doi.org/10.1029/2000JD000298

ATWOOD ET AL. 11 of 12



- Wallace, J. M., Rasmusson, E. M., Mitchell, T. P., Kousky, V. E., Sarachik, E. S., & von Storch, H. (1998). On the structure and evolution of ENSO-related climate variability in the tropical Pacific: Lessons from TOGA. *Journal of Geophysical Research*, 103(C7), 14241–14259. https://doi.org/10.1029/97JC02905
- Wang, Y. J., Cheng, H., Edwards, R. L., An, Z. S., Wu, J. Y., Shen, C. C., & Dorale, J. A. (2001). A high-resolution absolute-dated late Pleistocene monsoon record from Hulu Cave China. *Science*, 294(5550), 2345–2348. https://doi.org/10.1126/science.1064618
- Zhang, H., Griffiths, M. L., Chiang, J. C., Kong, W., Wu, S., Atwood, A., et al. (2019). East Asian hydroclimate modulated by the position of the westerlies during Termination I. Science, 362, 580–583.

References From the Supporting Information

- Bao, Q., Lin, P., Zhou, T., Liu, Y., Yu, Y., Wu, G., et al. (2013). The Flexible Global Ocean-Atmosphere-Land system model, Spectral Version 2: FGOALS-s2. Advances in Atmospheric Sciences, 30(3), 561–576. https://doi.org/10.1007/s00376-012-2113-9
- Colose, C. M., LeGrande, A. N., & Vuille, M. (2016). Hemispherically asymmetric volcanic forcing of tropical hydroclimate during the last millennium. *Earth System Dynamics*, 7(3), 681–696. https://doi.org/10.5194/esd-7-681-2016
- Gent, P. R., Danabasoglu, G., Donner, L. J., Holland, M. M., Hunke, E. C., Jayne, S. R., et al. (2011). The Community Climate System Model Version 4. *Journal of Climate*, 24(19), 4973–4991. https://doi.org/10.1175/2011JCLI4083.1
- Gordon, C., Cooper, C., Senior, C. A., Banks, H., Gregory, J. M., Johns, T. C., et al. (2000). The simulation of SST, sea ice extents and ocean heat transports in a version of the Hadley Centre coupled model without flux adjustments. *Climate Dynamics*, 16(2-3), 147–168. https://doi.org/10.1007/s003820050010
- Harrison, S. P., Bartlein, P. J., Brewer, S., Prentice, I. C., Boyd, M., Hessler, I., et al. (2014). Climate model benchmarking with glacial and mid-Holocene climates. *Climate Dynamics*. 43(3-4), 671–688. https://doi.org/10.1007/s00382-013-1922-6
- Iversen, T., Bentsen, M., Bethke, I., Debernard, J. B., Kirkevåg, A., Seland, Ø., et al. (2013). The Norwegian earth system model, NorESM1-M—Part 2: Climate response and scenario projections. *Geoscientific Model Development*, 6(2), 389–415. https://doi.org/10.5194/gmd-6-389-2013
- K-1-Model-Developers (2004) K-1 coupled GCM (MIROC) description. in K-1 technical report 1, eds H. Hasumi, S. Emori (Center for Climate System Research, University of Tokyo).
- Li, L., Lin, P., Yu, Y., Wang, B., Zhou, T., Liu, L., et al. (2013). The flexible global ocean-atmosphere-land system model, Grid-point Version 2: FGOALS-g2. Advances in Atmospheric Sciences, 30(3), 543–560. https://doi.org/10.1007/s00376-012-2140-6
- Marsland, S. J., Haak, H., Jungclaus, J. H., Latif, M., & Röske, F. (2003). The Max-Planck-Institute global ocean/sea ice model with orthogonal curvilinear coordinates. *Ocean Modelling*, 5(2), 91–127. https://doi.org/10.1016/S1463-5003(02)00015-X
- Marti, O., Braconnot, P., Bellier, J., Benshila, R., Bony, S., Brockmann, P., et al. (2005). The new IPSL climate system model: IPSL-CM4. Note du Pôle de Modélisation, IPSL, 26, 1–86.
- Otto-Bliesner, B. L., Brady, E. C., Clauzet, G., Tomas, R., Levis, S., & Kothavala, Z. (2006). Last Glacial Maximum and Holocene climate in CCSM3. *Journal of Climate*, 19(11), 2526–2544. https://doi.org/10.1175/JCLI3748.1
- Otto-Bliesner, B. L., Brady, E. C., & Fasullo, J. (2016). Climate variability and change since 850 CE: An ensemble approach with the community earth system model. *Bulletin of American Meteorological Society*, 97(5), 735–754. https://doi.org/10.1175/BAMS-D-14-00233.1
- Raddatz, T. J., Reick, C. H., Knorr, W., Kattge, J., Roeckner, E., Schnur, R., et al. (2007). Will the tropical land biosphere dominate the climate–carbon cycle feedback during the twenty-first century? *Climate Dynamics*, 29(6), 565–574. https://doi.org/10.1007/s00382-007-0247-8
- Roeckner, E. et al. (2003). The atmospheric general circulation model ECHAM5—Part I: Model description. In Max-Planck-Institut für Meteorologie, Technical Report.
- Rotstayn, L. D., Collier, M. A., Dix, M. R., Feng, Y., Gordon, H. B., O'Farrell, S. P., et al. (2010). Improved simulation of Australian climate and ENSO-related rainfall variability in a global climate model with an interactive aerosol treatment. *International Journal of Climatology*, 30, 1067–1088.
- Salas-Melia, D., Chauvin, M. D., Douville, H., Gueremy, J. F., Marquet, P., Planton, S., et al. (2005). Description and validation of the CNRM-CM3 global coupled model. CNRM working note, 103.
- Schmidt, G. A., Kelley, M., Nazarenko, L., Ruedy, R., Russell, G. L., Aleinov, I., et al. (2014). Configuration and assessment of the GISS ModelE2 contributions to the CMIP5 archive. *Journal of Advances in Modeling Earth Systems*, 6(1), 141–184. https://doi.org/10.1002/2013MS000265
- Schmidt, G. A., Ruedy, R., Hansen, J. E., Aleinov, I., Bell, N., Bauer, M., et al. (2006). Present-day atmospheric simulations using GISS ModelE: Comparison to in situ, satellite, and reanalysis data. *Journal of Climate*, 19(2), 153–192. https://doi.org/10.1175/JCLI3612.1
- Taylor, K. E., Stouffer, R. J., & Meehl, G. A. (2012). An overview of CMIP5 and the experiment design. Bulletin of the American Meteorological Society, 93(4), 485–498. https://doi.org/10.1175/BAMS-D-11-00094.1
- Voldoire, A., Sanchez-Gomez, E., Salas y Mélia, D., Decharme, B., Cassou, C., Sénési, S., et al. (2013). The CNRM-CM5.1 global climate model: description and basic evaluation. Climate Dynamics, 40(9-10), 2091–2121. https://doi.org/10.1007/s00382-011-1259-y
- Watanabe, S., Hajima, T., Sudo, K., Nagashima, T., Takemura, T., Okajima, H., et al. (2011). MIROC-ESM 2010: Model description and basic results of CMIP5-20c3m experiments. Geoscientific Model Development, 4(4), 845–872. https://doi.org/10.5194/gmd-4-845-2011
- Xin, X.-G., Wu, T.-W., & Zhang, J. (2013). Introduction of CMIP5 experiments carried out with the climate system models of Beijing Climate Center. *Advances in Climate Change Research*, 4, 41–49.
- Yongqiang, Y., Rucong, Y., Xuehong, Z., & Hailong, L. (2002). A flexible coupled ocean-atmosphere general circulation model. *Advances in Atmospheric Sciences*, 19(1), 169–190. https://doi.org/10.1007/s00376-002-0042-8
- Yukimoto, S., Adachi, Y., Hosaka, M., Sakami, T., Yoshimura, H., Hirabara, M., et al. (2012). A new global climate model of the meteorological research institute: MRI-CGCM3—Model description and basic performance. *Journal of the Meteorological Society of Japan. Ser. II*, 90A(0), 23–64. https://doi.org/10.2151/jmsj.2012-A02

ATWOOD ET AL. 12 of 12